Helsinki University of Technology Institute of Mathematics Research Reports
Espoo 2010 A595

NUMERICAL COMPUTATIONS WITH H(DIV)-FINITE ELEMENTS FOR THE BRINKMAN PROBLEM

Juho Könnö Rolf Stenberg

Aalto University

Helsinki University of Technology Institute of Mathematics Research Reports
Espoo 2010 A595

NUMERICAL COMPUTATIONS WITH H(DIV)-FINITE ELEMENTS FOR THE BRINKMAN PROBLEM

Juho Könnö **Rolf Stenberg**

Aalto University
School of Science and Technology
Department of Mathematics and Systems Analysis

Juho Könnö, Rolf Stenberg: *Numerical computations with H(div)-finite elements for the Brinkman problem*; Helsinki University of Technology Institute of Mathematics Research Reports A595 (2010).

Abstract: *The H(div)-conforming approach for the Brinkman equation is studied numerically, verifying the theoretical a priori and a posteriori analysis in [21, 22]. We also present a hybridization technique for the problem, complete with convergence analysis and numerical verication. In addition, diffent boundary conditions and their enforcing along with the applicability of the method to some subsurface flow problems is addressed.*

AMS subject classifications: 65N30

Keywords: Brinkman equation, H(div) conforming, SIPG, Nitsche, a posteriori, computations

Correspondence

Aalto University
Department of Mathematics and Systems Analysis
P.O. Box 11100
FI-00076 Aalto
Finland
jkonno@math.tkk.fi, rolf.stenberg@tkk.fi

Received 2010-11-25

ISBN 978-952-60-3511-6 (print) ISSN 0784-3143 (print)
ISBN 978-952-60-3512-3 (PDF) ISSN 1797-5867 (PDF)

Aalto University
School of Science and Technology
Department of Mathematics and Systems Analysis
P.O. Box 11100, FI-00076 Aalto, Finland
email: math@tkk.fi http://math.tkk.fi/

NUMERICAL COMPUTATIONS WITH $H(\mathrm{div})$-FINITE ELEMENTS FOR THE BRINKMAN PROBLEM

JUHO KÖNNÖ* AND ROLF STENBERG†

Abstract. The $H(\mathrm{div})$-conforming approach for the Brinkman equation is studied numerically, verifying the theoretical a priori and a posteriori analysis in [22, 23]. We also present a hybridization technique for the problem, complete with convergence analysis and numerical verification. In addition, diffent boundary conditions and their enforcing along with the applicability of the method to some subsurface flow problems is addressed.

1. Introduction. The Brinkman equation describes the flow of a viscous fluid in a highly porous medium. Mathematically the model is a parameter-dependent combination of the Darcy and Stokes models. For a derivation of and details on the Brinkman equations we refer to [25, 1, 2, 3, 30]. Typical applications of the model lie in subsurface flow problems, along with some special applications, such as heat pipes and composite manufacturing [21, 15]. The effects of taking the viscosity into account are most pronounced in the presence of large crack or vugs, typical of e.g. real-life oil reservoirs. The advantages of the parameter dependent model in reservoir simulation include the ability to perform computations in cracked domains without the exact knowledge of the crack locations, and not having to know the exact boundary condition between the free-flow and porous domains. The Brinkman model is also used as a coupling layer between a free surface flow and a porous Darcy flow [13]. Numerical results for the Brinkman flow have been previously presented for the Hsieh-Clough-Tocher element in [32], for the classical Stokes elements in [16, 11, 17], and for coupling the Stokes and Darcy flows with an SIPG method in [20]. For the $H(\mathrm{div})$-conforming approximation, numerical results with a subgrid algorithm can be found in [18].

The structure of the paper is as follows. In Chapter 2 we briefly recall the mathematical formulation of the model, and introduce the necessary function spaces. Chapter 3 carries on to introducing the $H(\mathrm{div})$-conforming finite element discretization for the problem, along with the Nitsche formulation for assuring conformity and stability in the discrete spaces. We also recall the main results of the a priori and a posteriori analysis carried out in [22], along with the postprocessing procedure necessary for the optimal convergence results.

Chapters 4 and 5 are related to two practical aspects of the implementation. In Chapter 4 we introduce a hybridization technique for the parameter dependent problem based on previous hybridization techniques for mixed and DG methods [12, 10, 8]. The practicability of the hybridization and the benefits therein are discussed briefly. Chapter 5 is devoted to techniques for enforcing the boundary conditions, which are non-trivial to assign for this parameter-dependent problem.

We end the paper with extensive numerical tests in Chapter 6. We first demonstrate the convergence rates predicted by the theory for both the relative error as well as the a posteriori indicator. Furthermore, the performance of the method is compared with that of a MINI finite element discretization. Next, the importance

*Department of Mathematics and Systems Analysis, Helsinki University of Technology, P.O. Box 1100, FIN-02015 TKK, Espoo, Finland (jkonno@math.tkk.fi). Supported by the Finnish Cultural Foundation.

†Department of Mathematics and Systems Analysis, Helsinki University of Technology, P.O. Box 1100, FIN-02015 TKK, Espoo, Finland (rolf.stenberg@tkk.fi).

of the postprocessing method is clarified and convergence of the hybridized method is studied. The weak enforcing of the boundary conditions and adaptive refinement techniques are studied in the framework of the classical Poisseuille flow. The chapter ends with a practical example of the Brinkman flow with actual material parameters from the SPE10 dataset [9].

2. The Brinkman model. Let $\Omega \subset \mathbb{R}^n$, with $n = 2, 3$, be a domain with a polygonal or polyhedral boundary. We denote by $\boldsymbol{u}$ the velocity field of the fluid and by p the pore pressure. The equations are scaled as presented in [16], with the single parameter t representing the effective viscosity of the fluid, which is assumed constant for simplicity. With this notation, the equations are

$$-t^2\Delta\boldsymbol{u} + \boldsymbol{u} + \nabla p = \boldsymbol{f}, \quad \text{in } \Omega, \tag{2.1}$$

$$\text{div } \boldsymbol{u} = g, \quad \text{in } \Omega. \tag{2.2}$$

For simplicity of the mathematical analysis, we consider homogenous Dirichlet boundary conditions for the velocity field. For $t > 0$ the boundary conditions are

$$\boldsymbol{u} = \boldsymbol{0}. \tag{2.3}$$

For the limiting case $t = 0$ we assume the boundary condition

$$\boldsymbol{u}\cdot\boldsymbol{n} = 0. \tag{2.4}$$

The enforcing of different boundary conditions is adressed in Chapter 5 in more detail.

For $t > 0$, the equations are formally a Stokes problem. The solution $(\boldsymbol{u}, p)$ is sought in $\boldsymbol{V} \times Q = [H_0^1(\Omega)]^n \times L_0^2(\Omega)$. For the case $t = 0$ we get the Darcy problem, and accordingly the solution space can be chosen as $\boldsymbol{V} \times Q = H(\text{div}, \Omega) \times L_0^2(\Omega)$ or $\boldsymbol{V} \times Q = [L^2(\Omega)]^n \times [H^1(\Omega) \cap L_0^2(\Omega)]$. Here, we focus on the first choice of spaces.

In the following, we denote by $(\cdot\,,\cdot)_D$ the standard L^2-inner product over a set $D \subset \mathbb{R}^n$. If $D = \Omega$, the subscript is dropped for convenience. Similarly, $\langle\cdot\,,\cdot\rangle_B$ is the L^2-inner product over an $(n-1)$-dimensional subset $B \subset \bar{\Omega}$. We define the following bilinear forms

$$a(\boldsymbol{u}, \boldsymbol{v}) = t^2(\nabla\boldsymbol{u}, \nabla\boldsymbol{v}) + (\boldsymbol{u}, \boldsymbol{v}), \tag{2.5}$$

$$b(\boldsymbol{v}, p) = -(\text{div } \boldsymbol{v}, p), \tag{2.6}$$

and

$$\mathcal{B}(\boldsymbol{u}, p; \boldsymbol{v}, q) = a(\boldsymbol{u}, \boldsymbol{v}) + b(\boldsymbol{v}, p) + b(\boldsymbol{u}, q). \tag{2.7}$$

The weak formulation of the Brinkman problem then reads: Find $(\boldsymbol{u}, p) \in \boldsymbol{V} \times Q$ such that

$$\mathcal{B}(\boldsymbol{u}, p; \boldsymbol{v}, q) = (\boldsymbol{f}, \boldsymbol{v}) - (g, q), \quad \forall(\boldsymbol{v}, q) \in \boldsymbol{V} \times Q. \tag{2.8}$$

3. Solution by mixed finite elements. Let $\mathcal{K}_h$ be a shape-regular partition of Ω into simplices. As usual, the diameter of an element K is denoted by h_K, and the global mesh size h is defined as $h = \max_{K\in\mathcal{K}_h} h_K$. We denote by $\mathcal{E}_h$ the set of all faces of $\mathcal{K}_h$. We write h_E for the diameter of a face E.

We introduce the jump and average of a piecewise smooth scalar function f as follows. Let $E = \partial K \cap \partial K'$ be an interior face shared by two elements K and K'. Then the jump of f over E is defined by

$$[\![f]\!] = f|_K - f|_{K'}, \tag{3.1}$$

and the average as

$$\{\!|f|\!\} = \frac{1}{2}(f|_K + f|_{K'}). \tag{3.2}$$

For vector valued functions, we define the jumps and averages analogously. In addition, we define the tangential component on each face as

$$\boldsymbol{u}_{\boldsymbol{\tau}} = \boldsymbol{u} - (\boldsymbol{u}\cdot\boldsymbol{n})\boldsymbol{n}, \tag{3.3}$$

in which $\boldsymbol{n}$ is the normal vector of the face in question.

3.1. The mixed method and the norms. Mixed finite element discretization of the problem is based on finite element spaces $\boldsymbol{V}_h \times Q_h \subset H(\mathrm{div},\Omega) \times L^2_0(\Omega)$ of piecewise polynomial functions with respect to $\mathcal{K}_h$. We will focus here on the Raviart-Thomas (RT) and Brezzi-Douglas-Marini (BDM) families of elements [8]. In three dimensions the counterparts are the Nédélec elements [27] and the BDDF elements [7]. That is, for an approximation of order $k \geq 1$, the flux space $\boldsymbol{V}_h$ is taken as one of the following two spaces

$$\boldsymbol{V}_h^{RT} = \{\boldsymbol{v} \in H(\mathrm{div},\Omega) \mid \boldsymbol{v}|_K \in [P_{k-1}(K)]^n \oplus \boldsymbol{x}\tilde{P}_{k-1}(K)\ \forall K \in \mathcal{K}_h\}, \tag{3.4}$$

$$\boldsymbol{V}_h^{BDM} = \{\boldsymbol{v} \in H(\mathrm{div},\Omega) \mid \boldsymbol{v}|_K \in [P_k(K)]^n\ \forall K \in \mathcal{K}_h\}, \tag{3.5}$$

where $\tilde{P}_{k-1}(K)$ denotes the homogeneous polynomials of degree $k-1$. The pressure is approximated in the same space for both choices of the velocity space, namely

$$Q_h = \{q \in L^2_0(\Omega) \mid q|_K \in P_{k-1}(K)\ \forall K \in \mathcal{K}_h\}. \tag{3.6}$$

Notice that $\boldsymbol{V}_h^{RT} \subset \boldsymbol{V}_h^{BDM}$. The combination of spaces satisfies the following equilibrium property:

$$\mathrm{div}\ \boldsymbol{V}_h \subset Q_h. \tag{3.7}$$

To assure the conformity and stability of the approximation, we use the an SIPG method [19, 28], also known as Nitsche's method, with a suitably chosen stabilization parameter $\alpha > 0$. We define the following mesh-dependent bilinear form

$$\mathcal{B}_h(\boldsymbol{u},p;\boldsymbol{v},q) = a_h(\boldsymbol{u},\boldsymbol{v}) + b(\boldsymbol{v},p) + b(\boldsymbol{u},q), \tag{3.8}$$

in which

$$a_h(\boldsymbol{u},\boldsymbol{v}) = (\boldsymbol{u},\boldsymbol{v}) + t^2\left[\sum_{K\in\mathcal{K}_h}(\nabla\boldsymbol{u},\nabla\boldsymbol{v})_K\right. \tag{3.9}$$

$$\left. + \sum_{E\in\mathcal{E}_h}\{\frac{\alpha}{h_E}\langle[\![\boldsymbol{u}_{\boldsymbol{\tau}}]\!],[\![\boldsymbol{v}_{\boldsymbol{\tau}}]\!]\rangle_E - \langle\{\!|\frac{\partial\boldsymbol{u}}{\partial n}|\!\},[\![\boldsymbol{v}_{\boldsymbol{\tau}}]\!]\rangle_E - \langle\{\!|\frac{\partial\boldsymbol{v}}{\partial n}|\!\},[\![\boldsymbol{u}_{\boldsymbol{\tau}}]\!]\rangle_E\}\right].$$

Then the discrete problem is to find $\boldsymbol{u}_h \in \boldsymbol{V}_h$ and $p_h \in Q_h$ such that

$$\mathcal{B}_h(\boldsymbol{u}_h, p_h; \boldsymbol{v}, q) = (\boldsymbol{f}, \boldsymbol{v}) - (g, q), \quad \forall (\boldsymbol{v}, q) \in \boldsymbol{V}_h \times Q_h. \tag{3.10}$$

We introduce the following mesh-dependent norms for the problem. For the velocity we use

$$\|\boldsymbol{u}\|_{t,h}^2 = \|\boldsymbol{u}\|_0^2 + t^2 \left[\sum_{K \in \mathcal{K}_h} \|\nabla \boldsymbol{u}\|_{0,K}^2 + \sum_{E \in \mathcal{E}_h} \frac{1}{h_E} \|[\![\boldsymbol{u}_{\boldsymbol{\tau}}]\!]\|_{0,E}^2 \right], \tag{3.11}$$

and for the pressure

$$|\!|\!| p |\!|\!|_{t,h}^2 = \sum_{K \in \mathcal{K}_h} \frac{h_K^2}{h_K^2 + t^2} \|\nabla p\|_{0,K}^2 + \sum_{E \in \mathcal{E}_h} \frac{h_E}{h_E^2 + t^2} \|[\![p]\!]\|_{0,E}^2. \tag{3.12}$$

Note that both of the norms are also parameter dependent. To show continuity, we use the somewhat stronger norm

$$\|\boldsymbol{u}\|_{t,*}^2 = \|\boldsymbol{u}\|_{t,h}^2 + t^2 \sum_{E \in \mathcal{E}_h} h_E \|\{\!\{\frac{\partial \boldsymbol{u}}{\partial n}\}\!\}\|_{0,E}^2. \tag{3.13}$$

It is easily shown that the norms (3.11) and (3.13) are equivalent in $\boldsymbol{V}_h$. We have the result [31], with $C_I > 0$.

$$h_E \|\frac{\partial \boldsymbol{v}}{\partial n}\|_{0,E}^2 \leq C_I \|\nabla \boldsymbol{v}\|_{0,K}^2, \quad \forall \boldsymbol{v} \in \boldsymbol{V}_h. \tag{3.14}$$

3.2. A priori analysis. For the proofs of the following results, see [22, 23]. First we note that the method is consistent.

THEOREM 3.1. *The exact solution* $(\boldsymbol{u}, p) \in \boldsymbol{V} \times Q$ *satisfies*

$$\mathcal{B}_h(\boldsymbol{u}, p; \boldsymbol{v}, q) = (\boldsymbol{f}, \boldsymbol{v}) - (g, q), \quad \forall (\boldsymbol{v}, q) \in \boldsymbol{V}_h \times Q_h. \tag{3.15}$$

In addition, the bilinear form $a_h(\cdot\,,\cdot)$ is coercive in $\boldsymbol{V}_h$ in the mesh-dependent norm (3.11).

LEMMA 3.2. *Let* C_I *be the constant from the inequality* (3.14). *For* $\alpha > C_I/4$ *there exists a positive constant* C *such that*

$$a_h(\boldsymbol{v}, \boldsymbol{v}) \geq C \|\boldsymbol{v}\|_{t,h}^2, \quad \forall \boldsymbol{v} \in \boldsymbol{V}_h. \tag{3.16}$$

Next, we recall the discrete Brezzi-Babuska stability condition.

LEMMA 3.3. *There exists a positive constant* C *such that*

$$\sup_{\boldsymbol{v} \in \boldsymbol{V}_h} \frac{b(\boldsymbol{v}, q)}{\|\boldsymbol{v}\|_{t,h}} \geq C |\!|\!| q |\!|\!|_{t,h}, \quad \forall q \in Q_h. \tag{3.17}$$

By the above stability results for $a_h(\cdot\,,\cdot)$ and $b(\cdot\,,\cdot)$ the following stability result holds, see e.g. [8].

LEMMA 3.4. *There is a positive constant* C *such that*

$$\sup_{(\boldsymbol{v}, q) \in \boldsymbol{V}_h \times Q_h} \frac{\mathcal{B}_h(\boldsymbol{r}, s; \boldsymbol{v}, q)}{\|\boldsymbol{v}\|_{t,h} + |\!|\!| q |\!|\!|_{t,h}} \geq C(\|\boldsymbol{r}\|_{t,h} + |\!|\!| s |\!|\!|_{t,h}), \quad \forall (\boldsymbol{r}, s) \in \boldsymbol{V}_h \times Q_h. \tag{3.18}$$

For interpolation in $H(\mathrm{div})$, a special interpolation operator $\boldsymbol{R}_h : H(\mathrm{div},\Omega) \to \boldsymbol{V}_h$ is required, see [8]. We denote by $P_h : L^2(\Omega) \to Q_h$ the L^2-projection. The interpolants possess the following properties:

$$(\mathrm{div}\ (\boldsymbol{v} - \boldsymbol{R}_h\boldsymbol{v}), q) = 0, \quad \forall q \in Q_h, \tag{3.19}$$

$$(\mathrm{div}\ \boldsymbol{v}, q - P_h q) = 0, \quad \forall \boldsymbol{v} \in \boldsymbol{V}_h, \tag{3.20}$$

and

$$\mathrm{div}\ \boldsymbol{R}_h = P_h \mathrm{div}. \tag{3.21}$$

By stability and consistency we have the following quasioptimal a priori result shown in [22].

THEOREM 3.5. *There is a positive constant C such that*

$$\|\boldsymbol{u} - \boldsymbol{u}_h\|_{t,h} + |\!|\!| P_h p - p_h |\!|\!|_{t,h} \le C \|\boldsymbol{u} - \boldsymbol{R}_h\boldsymbol{u}\|_{t,h}. \tag{3.22}$$

This contains a superconvergence result for $|\!|\!| p_h - P_h p |\!|\!|_{t,h}$, which implies that the pressure solution can be improved by local postprocessing. Assuming full regularity, we conclude the chapter with the following a priori estimate.

$$\|\boldsymbol{u} - \boldsymbol{u}_h\|_{t,h} + |\!|\!| P_h p - p_h |\!|\!|_{t,h} \le \begin{cases} C(h^k + th^{k-1})\|\boldsymbol{u}\|_k, & \text{for RT,} \\ C(h^{k+1} + th^k)\|\boldsymbol{u}\|_{k+1}, & \text{for BDM.} \end{cases} \tag{3.23}$$

3.3. Postprocessing method. We recall the postprocessing method proposed in [22] based on the ideas of [26]. We seek the postprocessed pressure in an augmented space $Q_h^* \supset Q_h$, defined as

$$Q_h^* = \begin{cases} \{q \in L_0^2(\Omega) \mid q|_K \in P_k(K)\ \forall K \in \mathcal{K}_h\}, & \text{for RT,} \\ \{q \in L_0^2(\Omega) \mid q|_K \in P_{k+1}(K)\ \forall K \in \mathcal{K}_h\}, & \text{for BDM.} \end{cases} \tag{3.24}$$

The postprosessing method is: Find $p_h^* \in Q_h^*$ such that

$$P_h p_h^* = p_h \tag{3.25}$$

$$(\nabla p_h^*, \nabla q)_K = (t^2 \Delta \boldsymbol{u}_h - \boldsymbol{u}_h + \boldsymbol{f}, \nabla q)_K, \quad \forall q \in (I - P_h) Q_h^*|_K. \tag{3.26}$$

We have the following a priori results, which show that given sufficient regularity, the postprocessed pressure converges with an optimal rate.

THEOREM 3.6. *For the postprocessed solution $(\boldsymbol{u}_h, p_h^*)$ it holds*

$$\|\boldsymbol{u} - \boldsymbol{u}_h\|_{t,h} + |\!|\!| p - p_h^* |\!|\!|_{t,h} \le C \inf_{q^* \in Q_h^*} \Big\{ \|\boldsymbol{u} - R_h\boldsymbol{u}\|_{t,h} + |\!|\!| p - q^* |\!|\!|_{t,h} \tag{3.27}$$

$$+ \Big(\sum_{K \in \mathcal{K}_h} \frac{h_K^2}{h_K^2 + t^2} \|\nabla q^* + \boldsymbol{R}_h\boldsymbol{u} - t^2 \Delta R_h \boldsymbol{u} - \boldsymbol{f}\|_{0,K}^2 \Big)^{1/2} \Big\}.$$

Assuming full regularity, we have the following optimal a priori result for the postprocessed problem.

THEOREM 3.7. *For the solution $(\boldsymbol{u}_h, p_h^*)$ of the postprocessed problem it holds*

$$\|\boldsymbol{u} - \boldsymbol{u}_h\|_{t,h} + |\!|\!| p - p_h^* |\!|\!|_{t,h} \le \begin{cases} C(h^k + th^{k-1})\|\boldsymbol{u}\|_k, & \text{for RT,} \\ C(h^{k+1} + th^k)\|\boldsymbol{u}\|_{k+1}, & \text{for BDM.} \end{cases} \tag{3.28}$$

3.4. A posteriori estimates. In this section we introduce a residual-based a posteriori estimator for the postprocessed solution. It should be noted that the postprocessing is vital for a properly functioning estimator. We divide the estimator into two distinct parts, one defined over the elements and one over the edges of the mesh. The elementwise and edgewise estimators are defined as

$$\eta_K^2 = \frac{h_K^2}{h_K^2+t^2}\| - t^2\Delta \boldsymbol{u}_h + \boldsymbol{u}_h + \nabla p_h^* - \boldsymbol{f}\|_{0,K}^2 + (t^2+h_K^2)\|g - P_h g\|_{0,K}^2, \tag{3.29}$$

$$\eta_E^2 = \frac{t^2}{h_E}\|[\![\boldsymbol{u}_{h,\boldsymbol{\tau}}]\!]\|_{0,E}^2 + \frac{h_E}{h_E^2+t^2}\|[\![t^2\frac{\partial \boldsymbol{u}_h}{\partial \boldsymbol{n}}]\!]\|_{0,E}^2 + \frac{h_E}{h_E^2+t^2}\|[\![p_h^*]\!]\|_{0,E}^2. \tag{3.30}$$

The global estimator is

$$\eta = \left(\sum_{K\in\mathcal{K}_h}\eta_K^2 + \sum_{E\in\mathcal{E}_h}\eta_E^2\right)^{1/2}. \tag{3.31}$$

Note that setting $t = 0$ gives the standard estimator for the Darcy problem, see e.g. [26, 24]. In the following, we address the reliability and efficiency of the estimator and show the terms of the estimator to be properly matched to one another.

The estimator introduced is both an upper and a lower bound for the actual error as shown by the following results, provided that a saturation assumption holds. For a proof, see [22].

THEOREM 3.8. *There exists a constant $C > 0$ such that*

$$\|\boldsymbol{u} - \boldsymbol{u}_h\|_{t,h} + |\!|\!|p - p_h^*|\!|\!|_{t,h} \le C\eta. \tag{3.32}$$

THEOREM 3.9. *There exists a constant $C > 0$ such that*

$$\begin{aligned}\eta^2 \le C\Big\{&\|\boldsymbol{u} - \boldsymbol{u}_h\|_{t,h}^2 + |\!|\!|p - p_h^*|\!|\!|_{t,h}^2 \\ &+ \sum_{K\in\mathcal{K}_h}\Big(\frac{h_K^2}{h_K^2+t^2}\|\boldsymbol{f} - \boldsymbol{f}_h\|_{0,K}^2 + (t^2+h_K^2)\|g - P_h g\|_{0,K}^2\Big)\Big\}.\end{aligned} \tag{3.33}$$

Thus for the displacement $\boldsymbol{u}_h$ and the postprocessed pressure p_h^* we have by Theorems 3.8 and 3.9 a reliable and efficient indicator for all values of the effective viscosity parameter t.

4. Hybridization. A well-known method for dealing with the indefinite system resulting in from the Darcy equation is the hybridization technique introduced in [5, 8]. The idea is to enforce the tangential continuity via Lagrange multipliers chosen suitably and relaxing the continuity requirement on the finite element space. Thus, we drop the normal continuity requirement in the spaces $\boldsymbol{V}_h^{BDM}$ and $\boldsymbol{V}_h^{RT}$ and denote these discontinuous counterparts by $\tilde{\boldsymbol{V}}_h$. In addition, we introduce the corresponding multiplier spaces

$$\Lambda_h^{BDM} = \{\lambda \in [L^2(\mathcal{E}_h)]^{n-1} \mid \lambda \in P_k(E),\ E\in\mathcal{E}_h,\ \lambda|_E = 0,\ E\subset\partial\Omega\}, \tag{4.1}$$

$$\Lambda_h^{RT} = \{\lambda \in [L^2(\mathcal{E}_h)]^{n-1} \mid \lambda \in P_{k-1}(E),\ E\in\mathcal{E}_h,\ \lambda|_E = 0,\ E\subset\partial\Omega\}, \tag{4.2}$$

in which $\mathcal{E}_h$ denotes the collection of all faces of the mesh. It can be easily shown, that the normal continuity of a discrete flux $\boldsymbol{u}_h \in \tilde{\boldsymbol{V}}_h$ is equivalent to the requirement

$$\sum_{K\in\mathcal{K}_h}\langle \boldsymbol{u}_h\cdot\boldsymbol{n}, \mu\rangle_{\partial K} = 0, \quad \forall \mu \in \Lambda_h. \tag{4.3}$$

Accordingly, the original finite element problem (3.10) can be hybridized in the following form: Find $(\boldsymbol{u}_h, p_h, \lambda_h) \in \tilde{\boldsymbol{V}}_h \times Q_h \times \Lambda_h$ such that

$$\mathcal{B}_h(\boldsymbol{u}_h, p_h; \boldsymbol{v}, q) + \sum_{K \in \mathcal{K}_h} \langle \boldsymbol{v} \cdot \boldsymbol{n}, \lambda_h \rangle_{\partial K} = (\boldsymbol{f}, \boldsymbol{v}) + (g, q), \tag{4.4}$$

$$\sum_{K \in \mathcal{K}_h} \langle \boldsymbol{u}_h \cdot \boldsymbol{n}, \mu \rangle_{\partial K} = 0 \tag{4.5}$$

for all $(\boldsymbol{v}, q, \mu) \in \tilde{\boldsymbol{V}}_h \times Q_h \times \Lambda_h$. Due to (4.3), the solution $(\boldsymbol{u}_h, p_h)$ of the hybridized system coincides with that of the original system. Thus, we need not modify the postprocessing procedure even if we drop the continuity requirement from the velocity space.

4.1. Hybridization of the Nitsche term. However, now the matrix block corresponding to the bilinear form $\mathcal{B}_h(\boldsymbol{u}_h, p_h; \boldsymbol{v}, q)$ is a block diagonal system only for the special case $t = 0$, and for a non-zero effective viscosity we cannot eliminate the variables locally. To alleviate this problem we introduce a second hybrid variable for the Nitsche term of the velocity, see e.g. [10]. Recall, that the velocity-velocity term of the bilinear form $\mathcal{B}_h(\boldsymbol{u}_h, p_h; \boldsymbol{v}, q)$ is

$$a_h(\boldsymbol{u}, \boldsymbol{v}) = (\boldsymbol{u}, \boldsymbol{v}) + t^2 \left[\sum_{K \in \mathcal{K}_h} (\nabla \boldsymbol{u}, \nabla \boldsymbol{v})_K \right. \tag{4.6}$$

$$\left. + \sum_{E \in \mathcal{E}_h} \{ \frac{\alpha}{h_E} \langle [\![\boldsymbol{u}_{\boldsymbol{\tau}}]\!], [\![\boldsymbol{v}_{\boldsymbol{\tau}}]\!] \rangle_E - \langle \{\!\{ \frac{\partial \boldsymbol{u}}{\partial n} \}\!\}, [\![\boldsymbol{v}_{\boldsymbol{\tau}}]\!] \rangle_E - \langle \{\!\{ \frac{\partial \boldsymbol{v}}{\partial n} \}\!\}, [\![\boldsymbol{u}_{\boldsymbol{\tau}}]\!] \rangle_E \} \right].$$

To this end, we follow [12], and formally introduce the mean value of $\boldsymbol{u}_{\boldsymbol{\tau}}$ as a new variable, $\boldsymbol{m} = \frac{1}{2}(\boldsymbol{u}_{1,\boldsymbol{\tau}} + \boldsymbol{u}_{2,\boldsymbol{\tau}})$. Thus we can write the tangential jump as

$$[\![\boldsymbol{u}_{\boldsymbol{\tau}}]\!] = 2(\boldsymbol{u}_{1,\boldsymbol{\tau}} - \boldsymbol{m}) = -2(\boldsymbol{u}_{2,\boldsymbol{\tau}} - \boldsymbol{m}). \tag{4.7}$$

Now using the new hybrid variables the bilinear form $a_h(\boldsymbol{u}, \boldsymbol{v})$ can be rewritten as

$$a_h(\boldsymbol{u}, \boldsymbol{m}; \boldsymbol{v}, \boldsymbol{r}) = (\boldsymbol{u}, \boldsymbol{v}) + t^2 \sum_{K \in \mathcal{K}_h} \{ (\nabla \boldsymbol{u}, \nabla \boldsymbol{v})_K + \frac{2\alpha}{h_E} \langle \boldsymbol{u}_{\boldsymbol{\tau}} - \boldsymbol{m}, \boldsymbol{v}_{\boldsymbol{\tau}} - \boldsymbol{r} \rangle_{\partial K}$$

$$- \langle \frac{\partial \boldsymbol{u}}{\partial n}, \boldsymbol{v}_{\boldsymbol{\tau}} - \boldsymbol{r} \rangle_{\partial K} - \langle \frac{\partial \boldsymbol{v}}{\partial n}, \boldsymbol{u}_{\boldsymbol{\tau}} - \boldsymbol{m} \rangle_{\partial K} \}.$$

Here, the hybrid variable $\boldsymbol{m}$ belongs to a space $\mathcal{M}_h \subset [L^2(\mathcal{E}_h)]^n$, the choice of which will be discussed subsequently. In addition, we introduce a slightly modified version of the norm (3.11) to encompass both the velocity and the hybrid variable:

$$\|(\boldsymbol{u}, \boldsymbol{m})\|_{t,h}^2 = \|\boldsymbol{u}\|_0^2 + t^2 \left[\sum_{K \in \mathcal{K}_h} \|\nabla \boldsymbol{u}\|_{0,K}^2 + \sum_{E \in \mathcal{E}_h} \frac{1}{h_E} \|\boldsymbol{u}_{\boldsymbol{\tau}} - \boldsymbol{m}\|_{0,E}^2 \right]. \tag{4.8}$$

Since for the exact solution the jumps disappear, the bilinear form is consistent. Using exactly the same arguments as those presented in [12] for (3.16), we have

LEMMA 4.1. *The hybridized bilinear form $a_h(\cdot, \cdot; \cdot, \cdot)$ is coercive in the discrete spaces $\boldsymbol{V}_h \times \mathcal{M}_h$, that is there exists a positive constant C such that*

$$a_h(\boldsymbol{v}, \boldsymbol{m}; \boldsymbol{v}, \boldsymbol{m}) \geq C \|(\boldsymbol{v}, \boldsymbol{m})\|_{t,h}^2, \quad \forall (\boldsymbol{v}, \boldsymbol{m}) \in \boldsymbol{V}_h \times \mathcal{M}_h. \tag{4.9}$$

Note, that the stability holds for any choice of the space $\mathcal{M}_h$. For complicated problems, this gives great flexibility. Thus, due to consistency and stability, we get optimal convergence rate as long as the space $\mathcal{M}_h$ is rich enough. Here we choose

$$\mathcal{M}_h = \{\boldsymbol{m} \in [L^2(\mathcal{E}_h)]^n \mid Q(E)\boldsymbol{m}|_E \in [P_k(E)]^{n-1}, \quad \forall E \in \mathcal{E}_h\}, \tag{4.10}$$

in which $Q(E)$ is the coordinate transformation matrix from the global n-dimensional coordinate system to the local $(n-1)$-dimensional coordinate system on the face E. Let $\boldsymbol{P}_h : [L^2(E)]^{n-1} \to \mathcal{M}_h$ be the L^2 projection on the faces. We then get the following interpolation estimate.

LEMMA 4.2. *Let $\boldsymbol{u} \in H^1(\Omega)$ be such that $\boldsymbol{u}|_K \in H^{s+1}(K)$ for $\frac{1}{2} < s \leq k$. Then it holds*

$$\|(\boldsymbol{u} - \boldsymbol{R}_h\boldsymbol{u}, \boldsymbol{u}_{\boldsymbol{\tau}} - \boldsymbol{P}_h\boldsymbol{u}_{\boldsymbol{\tau}})\|_{t,h} \leq C(h^{s+1} + th^s)\|\boldsymbol{u}\|_{s+1}. \tag{4.11}$$

Proof. We proceed by direct computation. Scaling and the Bramble-Hilbert lemma [6] yield

$$\begin{aligned}
\|(\boldsymbol{u} - \boldsymbol{R}_h\boldsymbol{u}, \boldsymbol{u}_{\boldsymbol{\tau}} - \boldsymbol{P}_h\boldsymbol{u}_{\boldsymbol{\tau}})\|_{t,h}^2 &\leq \|\boldsymbol{u} - \boldsymbol{R}_h\boldsymbol{u}\|_0^2 + t^2 \left[\sum_{K \in \mathcal{K}_h} \|\nabla(\boldsymbol{u} - \boldsymbol{R}_h\boldsymbol{u})\|_{0,K}^2 \right. \\
&\left. + \sum_{E \in \mathcal{E}_h} \{\frac{1}{h_E}\|(\boldsymbol{u} - \boldsymbol{R}_h\boldsymbol{u})_{\boldsymbol{\tau}}\|_{0,E}^2 + \frac{1}{h_E}\|(\boldsymbol{u}_{\boldsymbol{\tau}} - \boldsymbol{P}_h\boldsymbol{u}_{\boldsymbol{\tau}})\|_{0,E}^2\} \right] \\
&\leq C \left(h^{2s+2}\|\boldsymbol{u}\|_{s+1}^2 + t^2 \sum_{K \in \mathcal{K}_h} \{h_K^{2s}\|\boldsymbol{u}\|_{s+1,K}^2 + h_K^{2s}\|\boldsymbol{u}_{\boldsymbol{\tau}}\|_{s+1/2,K}^2\} \right).
\end{aligned}$$

The result is immediate after taking the square root. ∎

Combining the interpolation results with the consistency and ellipticity properties yields an optimal convergence rate for the velocity.

THEOREM 4.3. *Assuming sufficient regularity, for the finite element solution $(\boldsymbol{u}_h, \boldsymbol{m}_h)$ of the hybridized system it holds*

$$\|(\boldsymbol{u} - \boldsymbol{u}_h, \boldsymbol{u}_{\boldsymbol{\tau}} - \boldsymbol{m}_h))\|_{t,h} \leq C(h^{s+1} + th^s)\|\boldsymbol{u}\|_{s+1}. \tag{4.12}$$

The residual a posteriori estimator of Section 3.4 can be modified to handle the hybrid variable by modifying the edgewise estimator of (3.30) as follows

$$\eta_E^2 = \frac{t^2}{h_E}\|\boldsymbol{u}_{h,\boldsymbol{\tau}} - \boldsymbol{m}_h\|_{0,E}^2 + \frac{h_E}{h_E^2 + t^2}\|[\![t^2\frac{\partial \boldsymbol{u}_h}{\partial \boldsymbol{n}}]\!]\|_{0,E}^2 + \frac{h_E}{h_E^2 + t^2}\|[\![p_h^*]\!]\|_{0,E}^2. \tag{4.13}$$

Following the lines of [22, 23] it is easy to prove that also the modified estimator is both sharp and reliable. This will be demonstrated in numerical experiments in Section 6.

4.2. Implementation and local condensation. In practice, it is beneficial to choose the hybrid variable $\boldsymbol{m}$ slightly differently, namely as the weighted average $\boldsymbol{m} = \frac{t}{2}(\boldsymbol{u}_{1,\boldsymbol{\tau}} + \boldsymbol{u}_{2,\boldsymbol{\tau}})$. Now the hybridized bilinear form can be written as

$$
\begin{aligned}
a_h(\boldsymbol{u},\boldsymbol{m};\boldsymbol{v},\boldsymbol{r}) &= (\boldsymbol{u},\boldsymbol{v}) + \sum_{K\in\mathcal{K}_h} \frac{2\alpha}{h_E}\langle \boldsymbol{m},\boldsymbol{r}\rangle_{\partial K} \\
&+ t\sum_{K\in\mathcal{K}_h} \{\langle \frac{\partial \boldsymbol{u}}{\partial n},\boldsymbol{r}\rangle_{\partial K} + \langle \frac{\partial \boldsymbol{v}}{\partial n},\boldsymbol{m}\rangle_{\partial K} - \frac{2\alpha}{h_E}\langle \boldsymbol{u}_{\boldsymbol{\tau}},\boldsymbol{r}\rangle_{\partial K} - \frac{2\alpha}{h_E}\langle \boldsymbol{v}_{\boldsymbol{\tau}},\boldsymbol{m}\rangle_{\partial K}\} \\
&+ t^2\sum_{K\in\mathcal{K}_h} \{(\nabla \boldsymbol{u},\nabla \boldsymbol{v})_K + \frac{2\alpha}{h_E}\langle \boldsymbol{u}_{\boldsymbol{\tau}},\boldsymbol{v}_{\boldsymbol{\tau}}\rangle_{\partial K} - \langle \frac{\partial \boldsymbol{u}}{\partial n},\boldsymbol{v}_{\boldsymbol{\tau}}\rangle_{\partial K} - \langle \frac{\partial \boldsymbol{u}}{\partial n},\boldsymbol{u}_{\boldsymbol{\tau}}\rangle_{\partial K}\}.
\end{aligned}
$$

Note, that now we get a t-independent part for the hybrid variable and the system remains solvable even in the limit $t \to 0$. It is clear that all of the results in Section 4.1 hold also for the scaled hybrid variable.

The main motivation for the hybridization procedure is to break all connections in the original saddlepoint system to allow for local elimination of the velocity and pressure variables at the element level. After hydridization the matrix system gets the following form where A is the matrix corresponding to the bilinear form $a_h(\cdot,\cdot)$, B to $b(\cdot,\cdot)$, whilst C and D represent the connecting blocks for the hybrid variables for normal continuity and the Nitsche terms, respectively. M is the mass matrix for the Nitsche hybrid variable.

$$
\begin{pmatrix} A & B^T & C^T & D^T \\ B & 0 & 0 & 0 \\ C & 0 & 0 & 0 \\ D & 0 & 0 & M \end{pmatrix}. \tag{4.14}
$$

Since A and B are now block diagonal matrices, they can be inverted on the element level and we get the following symmetric and positive definite system for the hybrid variables. We denote the by H the following matrix that can be computed elementwise.

$$
H := A^{-1}B^T(BA^{-1}B^T)^{-1}BA^{-1} - A^{-1}. \tag{4.15}
$$

The matrix H is positive definite and symmetric. Eliminating the velocity and pressure from the system matrix (4.14) yields the following system matrix for the hybrid variables $(\lambda, \boldsymbol{m})$ corresponding to the normal continuity and tangential jumps, respectively.

$$
\begin{pmatrix} CHC^T & CHD^T \\ DHC^T & DHD^T + M \end{pmatrix}. \tag{4.16}
$$

Evidently the resulting system is symmetric and positive definite. Note, that whilst the connecting block D will vanish as $t \to 0$, the M block does not depend on t, thus the whole system remains invertible even in the limit.

The hybridized formulation is well-suited to solving large problems with the domain decomposition method. The hybrid variables readily form a discretization for the skeleton of the domain decomposition method for any choice of non-overlapping blocks. The local problems are of the Dirichlet type, and the domain decomposition method can be implemented easily using local solvers on the subdomains. We also have great flexibility in the choice of the hybridized variables, thus allowing one to use a lower number of degrees of freedom on the skeleton when computational resources are limited. Furthermore, only the skeleton of the domain decomposition mesh can be hybridized using e.g. direct solvers for the saddle point system in the subdomains.

5. Handling the boundary conditions. Since the Brinkman equation is a combination of the Darcy and Stokes equations, a variety of boundary conditions can be applied. Furthermore, some restrictions apply regarding which boundary conditions can be applied simultaneously.

5.1. Enforcing the pressure. A typical physical situation in which one desires to set the pressure on parts of the boundary is setting a pressure difference across the opposite ends of the computational domain. As a practical example, one might want to impose a pressure difference between an injection and a production well in a reservoir simulation. Note, that whereas it is possible to set the pressure on the whole of $\partial\Omega$ for the Darcy problem in the case $t = 0$, this alone is not a sound boundary condition for the Stokes-type problem with $t > 0$. Since the current formulation is based on the dual mixed Poisson problem, the pressure boundary condition now appears as a natural boundary condition. Then the pressure $p|_{\Gamma_p} = p_D$ can be set on $\Gamma_p \subset \partial\Omega$ by adding the following term to the loading:

$$\langle \boldsymbol{v}\cdot\boldsymbol{n}, p_D\rangle_{\Gamma_p}. \tag{5.1}$$

5.2. Enforcing the normal velocity. For the underlying Darcy problem, the essential boundary condition is the normal component of the velocity. Physically, this corresponds to prescribing the in- or outflow on the boundary. In the standard formulation, the boundary conditions must be set exactly into the finite element space with condensation. When using the hybrid formulation, however, setting the normal component corresponds to fixing the value of the Lagrange multiplier for the multipliers residing on the boundary. Thus we can simply add the Dirichlet data $\boldsymbol{u}\cdot\boldsymbol{n} = \boldsymbol{u}_D\cdot\boldsymbol{n}$ into the loading term for the Lagrange multiplier as follows:

$$\langle \boldsymbol{u}_D\cdot\boldsymbol{n}, \mu\rangle_{\Gamma_{\boldsymbol{u}\cdot\boldsymbol{n}}} \tag{5.2}$$

5.3. Enforcing the tangential velocity. For the case of a viscous flow, also the tangential component of the velocity can be prescribed on the boundary. The physical meaning is that of defining the allowed amount of slip for the fluid on the boundary. Since the nature of the problem is parameter dependent, it makes sense to enforce the tangential boundary condition weakly using the same Nitsche-type approach as for the internal tangential continuity. Denote by $\mathcal{E}_{h,\boldsymbol{u}_\tau}$ the collection of edges residing on the part of the boundary $\Gamma_{\boldsymbol{u}_\tau} \subset \partial\Omega$. To set the tangential velocity we add the following term to the bilinear form $a_h(\cdot\,,\cdot\,)$.

$$t^2 \sum_{E\in\mathcal{E}_{h,\boldsymbol{u}_\tau}} \{\frac{\alpha}{h_E}\langle \boldsymbol{u}_\tau, \boldsymbol{v}_\tau\rangle_E - \langle\frac{\partial \boldsymbol{u}}{\partial n}, \boldsymbol{v}_\tau\rangle_E - \langle\frac{\partial \boldsymbol{v}}{\partial n}, \boldsymbol{u}_\tau\rangle_E\}. \tag{5.3}$$

The loading is augmented by the term

$$t^2 \sum_{E\in\mathcal{E}_{h,\boldsymbol{u}_\tau}} \{\frac{\alpha}{h_E}\langle \boldsymbol{u}_{D,\tau}, \boldsymbol{v}_\tau\rangle_E - \langle\frac{\partial \boldsymbol{v}}{\partial n}, \boldsymbol{u}_{D,\tau}\rangle_E\}. \tag{5.4}$$

Note, that we need not separately hybridize the boundary degrees of freedom, since enforcing the boundary condition via Nitsche's method only involves degrees of freedom from each individual element and the A matrix retains its block structure.

6. Numerical tests. In this section, we shall numerically demonstrate the performance of the method. First, we test the convergence of the solution along with the performance of the a posteriori estimator in two cases with different regularity properties. The proposed method is also compared with the Stokes-type approach using the MINI element. We proceed to demonstrate the effect and the importance of the postprocessing procedure. Next, the convergence of the hybridized method is studied. Our fourth test is the classical Poisseuille flow, demonstrating the performance of Nitsche's method in assigning the boundary conditions and the applicability of the error indicator to adaptive mesh refinement. We end the section with a realistic example employing permeability data from the SPE10 dataset. In all of the test cases the ratio h/t is the ratio $1/(t\sqrt{N})$, in which N is the number of degrees of freedom. For a uniform mesh we have $h/t \approx 1/(t\sqrt{N})$. Note, that this holds only in the two-dimensional case considered in the computations. The data approximation term in the a posteriori estimator is neglected in the computations.

6.1. Convergence tests. For the purpose of testing the convergence rate, we pick a pressure p such that ∇p is a harmonic function. Thus, $\boldsymbol{u} = \nabla p$ is a solution of the problem for every $t \geq 0$. In polar coordinates (r, Θ) the pressure is chosen as

$$p(r, \Theta) = r^{\beta} \sin(\beta\Theta) + C. \tag{6.1}$$

The constant C is chosen such that the pressure will have a zero mean value. Moreover, we have $p \in H^{1+\beta}(\Omega)$, and subsequently $\boldsymbol{u} \in [H^{\beta}(\Omega)]^n$, see [14]. In the following, we have tested the convergence with a wide range of different parameter values, and the results are plotted with respect to the ratio of the viscosity parameter t to the mesh size h. Our aim is to demonstrate numerically, that the change in the nature of the problem indeed occurs at $t = h$, and that the convergence rates are optimal in both of the limiting cases. First we choose $\beta = 3.1$ to test the convergence rates in a smooth situation. With the first-order BDM element we are expecting h^2 converge in the Darcy end of the parameter range and h in the Stokes limit.

As is visible from the results in Figures 1 and 2, the behaviour of the problem changes numerically when $t = h$. Thus, even though in practical applications almost always $t > 0$, numerically the problem behaves like the Darcy problem when $t < h$. As can be seen from Figure 2, the converge rates follow quite closely those given by the theory. Furthermore, both the actual error and the a posteriori indicator behave in a similar manner. Notice, that the convergence rate exhibits a slight dip at the point in which the nature of the problem changes. However, since all of the a priori results are asymptotic, one notices that the optimal convergence rate is regained as soon as the mesh is refined.

To show the applicability of the a posteriori indicator to mesh refinement, we consider the more irregular case $\beta = 1.52$. Our refinement strategy consists of refining those elements in which the error exceeds 50 percent of the average value. The treshold is halved until at least five percent of the elements have been refined. The edge estimators are shared evenly between the neighbouring elements. Figure 6 shows, that the converge is considerably faster with adaptive refinement, as opposed to uniform refinement in Figure 4. Furthermore, adaptive refinement seems to alleviate the problem of convergence rate drop at the numerical turning point $t = h$. Clearly these results indicate that the a posteriori indicator proposed gives reasonable local bounds and can thus be used in adaptive mesh refinement.

6.2. Comparison with the MINI element. A common choice for solving the Stokes problem is the classical MINI element [4]. This element has been applied to

the Brinkman problem and thoroughly analyzed both theoretically and numerically in [19, 16]. We use the same test case as above with the regularity parameter set to $\beta = 3.1$. Notice, that the mesh-dependent norms (3.11) and (3.12) reduce to the ones presented in [19] when a continuous velocity-pressure pair is inserted. Thus we can use the same mesh-dependent norm for computing the error for both of the elements and the results are comparable with one another.

As can be seen from the results in Figure 8, the convergence rate for the MINI element is as expected of the order h throughout the parameter regime. For the BDM1 element, on the other hand, we get h^2 convergence in the Darcy regime, and after a slight dip at the turnaround point convergence relative to h. Turning our attention to Figure 7 reveals that the behaviour of the absolute value of the relative error differs vastly for the two elements. Clearly, the BDM element outperforms the MINI element in the Darcy regime by several decades of magnitude, whereas in the Stokes regime the performance of the MINI element is superior. This implicates that it is impossible to clearly tell which element is superior for the Brinkman flow. However, usually real-life reservoirs consist mostly of porous stone with scattered vugs and cracks. Thus the volume of the Stokes-type regime is often small compared to the Darcy regime, implying that the good performance of the BDM element in its natural operation conditions might offer significant performance increase for the overall simulation. In problems with a greater fraction of void space, such as filters with large free-flow areas separated by permeable thin layers, the Stokes-based elements might be a more natural choice.

6.3. Postprocessing. In this section, we show the necessity of the postprocessing by comparing the behaviour of both the exact error and the a posteriori estimator for the original and the postprocessed pressure. We shall use the same test case as in the previous sections. First we choose $\beta = 3.1$ for testing the effect on convergence and on the second run we choose $\beta = 1.52$ and use the same mesh refinement strategy to show the necessity of the post-processing for the usefulness of the error estimator.

From the results of Figure 9, it is immediately evident, that in the case of a small parameter t corresponding to a Darcy-type porous flow the postprocessing procedure is of vital importance for the method to work. However, as the viscosity increases the weighting of the pressure error changes, and the norm is more tolerable of variations in the pressure. Once again, this change in behaviour appears exactly at $t = h$. As regards convergence rate, the non-postprocessed method is able to attain close-to-optimal rate in the Stokes regime, cf. Figure 10. The same pattern is evident also with the more irregular test case with $\beta = 1.52$ as shown in Figure 11. When in the Darcy regime, the indicator simply does not work in adaptive refinement since the pressure solution lacks the necessary extra accuracy. However, when crossing into the Stokes regime, convergence starts to occur, and the adaptive procedure achieves a rather high rate of convergence.

Evidently, postprocessing is vital for the method in the Darcy regime. Even though the method seems to work without postprocessing in the Stokes regime, one cannot guarantee convergence and thus the method should always be used only in conjunction with the postprocessing scheme for the pressure. The cost of solving the postprocessed pressure is negligible compared to the total workload since the procedure is performed elementwise. Moreover, with postprocessing, using the BDM family of elements is more economical than using the RT family with respect to the number of degrees of freedom, since we can use initially one order lower approximation for the pressure, and still get the same order of polynomial approximation and convergence

after the postprocessing procedure.

6.4. Hybridized method. Here we study the convergence of the fully hybridized method for different parameter values using the modified norm (4.8) and the a posteriori estimator (4.13). We employ once again the same exact solution as in the other convergence tests with the regularity parameter β. As Figures 13 to 16 clearly show, the hybridized method behaves in an identical manner compared to the standard formulation, both in the case of a regular and an irregular exact solution. Thus it can be concluded that the error induced by hybridizing the jump terms inexactly is negligible. In Tables 6.1 and 6.2 we compare the condition numbers of the resulting linear systems for solving $(\boldsymbol{u}, p)$ and $(\lambda, \boldsymbol{m})$, respectively. The results are computed on identical meshes.

TABLE 6.1
Condition number for different values of t for the original system.

	DOF	$t = 0.01$	$t = 1$	$t = 10$
Initial mesh	348	0.66×10^3	1.17×10^8	1.55×10^{11}
First refinement	1352	3.85×10^3	4.16×10^9	9.92×10^{12}
Second refinement	5328	5.24×10^4	1.63×10^{11}	5.14×10^{14}

TABLE 6.2
Condition number for different values of t for the hybridized system.

	DOF	$t = 0.01$	$t = 1$	$t = 10$
Initial mesh	532	1.66×10^5	1.54×10^5	1.00×10^7
First refinement	2048	2.42×10^6	2.07×10^6	4.98×10^7
Second refinement	8032	3.67×10^7	3.06×10^7	2.67×10^8

From Table 6.1 we clearly see, that the condition number of the original saddlepoint system is rather sensitive to the parameter value. This is alleviated by the hybridization, but on the other hand we see that the condition number is higher than that of the original system for small values of the effective viscosity. For both methods the condition number appears to be relatively mesh-insensitive. In Figures 17 and 18 we plot the sparsity pattern of the final system matrix for both of the methods.

6.5. Poisseuille flow. The Poisseuille flow is a classical test case for which the exact solution is known. The setup represents a viscous flow in a long, narrow channel. The flow is driven by a linear pressure drop with no-slip boundary conditions for $t > 0$. For the Darcy case $t = 0$, only the normal component of the velocity vanishes on the boundary. We will test the convergence with Nitsche's method for the tangential boundary condition with adaptive mesh refinement. In the unit square we take the pressure to be $p = -x + \frac{1}{2}$. Then zero boundary conditions for the velocity give the exact solution $\boldsymbol{u} = (u, 0)$, with the x-directional velocity given by

$$u = \begin{cases} (1 + e^{1/t} - e^{(1-y)/t} - e^{y/t})/(1 + e^{1/t}), & t > 0 \\ 1, \quad t = 0. \end{cases} \tag{6.2}$$

As Figures 19 through 23 demonstrate, the adaptive process is able to catch the boundary layer effectively, leading to nearly identical converge rates for different parameter values as indicated by Figure 24. Note, that as the mesh is refined on the

edges, the problem changes numerically to a Stokes-type problem near the boundary since the mesh size h drops locally below the parameter t.

6.6. Example with realistic material parameters. In this final section we consider the Society of Petroleum Engineers test case SPE10 [9] with realistic porosity and permeability data for an oil reservoir. Instead of the simplified rescaled mathematical model problem (2.1), we now use the full Brinkman model with $\boldsymbol{K}$ denoting the symmetric permeability tensor and μ and $\tilde{\mu}$ are the dynamic and effective viscosities of the fluid, respectively. With this notation the problem reads [30, 29]

$$-\tilde{\mu}\Delta\boldsymbol{u} + \mu\boldsymbol{K}^{-1}\boldsymbol{u} + \nabla p = \boldsymbol{f}, \quad \text{in } \Omega, \tag{6.3}$$

$$\operatorname{div} \boldsymbol{u} = g, \quad \text{in } \Omega. \tag{6.4}$$

Following [29], we make the common choice $\tilde{\mu} = \mu$. We consider a single layer flow as a two-dimensional flow problem. For the outflow quantities to have meaningful units, we assume a thickness of 2 ft for the layer. The dimensions of the problem are 2200×1200 ft, viscosity is 100 cP. The flow is driven by a pressure of 0.01 atm on the left-hand side of the domain. The parameters are chosen such that the flow remains laminar in the piercing streak. The top and bottom boundaries have a no-flow boundary condition. To demonstrate the effect of the Brinkman term to the flow, we modify the permeability data by adding a rectangular streak of very high permeability with the dimensions 1100×20 ft in the middle of the domain, cf. Figures 25 and 26. The advantage of the Brinkman model is the ability to model cracks or vugs by simply assigning a very high (or infinite) permeability to these parts of the domain. In Figure 27 the velocity field for the non-modified problem is plotted. Comparing to Figure 28 we see that the flow is considerably diverted due to the internal high permeability area, e.g. a sand-filled crack, in the domain.

We compute the total flux through the two-dimensional field for different values of permeability for the streak. In addition, we extend the streak to run through the whole domain and study the total flow values through the domain for different streak permeabilities for both the Brinkman and Darcy models. The computations are performed on a triangular mesh with 33400 triangles and a total of 134020 degrees of freedom, which is refined once around the high-permeability streak.

TABLE 6.3
Total flow through the domain for varying permeability values of the streak.

	Streak permeability (D)	Brinkman (bbl/day)	Darcy (bbl/day)
Original		2.154×10^{-6}	2.154×10^{-6}
Internal streak	$K = 1.0 \times 10^{6}$	2.386×10^{-6}	2.386×10^{-6}
	$K = 1.0 \times 10^{12}$	2.386×10^{-6}	2.386×10^{-6}
	$K = 1.0 \times 10^{16}$	2.386×10^{-6}	2.386×10^{-6}
	$K = 1.0 \times 10^{100}$	2.386×10^{-6}	2.436×10^{-8}
Piercing streak	$K = 1.0 \times 10^{6}$	1.953×10^{1}	1.953×10^{1}
	$K = 1.0 \times 10^{12}$	6.133×10^{5}	1.918×10^{7}
	$K = 1.0 \times 10^{16}$	6.396×10^{5}	1.729×10^{11}

From the results it is clear that in the case of an internal streak both models give equivalent results. However, it should be kept in mind that for arbitrarily high values of permeability the Darcy system becomes ill-conditioned, whereas in the Brinkman model one can assign even infinite permeabilities and keep the system solvable, as demonstrated by choosing a permeability of 10^{100} D.

With the piercing streak the flow rates vary significantly when the flow in the streak crosses into the Stokes regime. Clearly, the Darcy equation overestimates the flow by several decades since it does not take the viscosity into account, whereas the Brinkman flow stagnates to a value limited by the viscosity of the fluid.

7. Conclusions. We were able to numerically demonstrate the theoretical results for the Darcy-based method of [22] for solving the Brinkman equation. Furthermore a hybridization technique was introduced for the whole system, which might prove useful for handling very large systems with domain decomposition or multiscale mixed finite element methods. The hybridized method was also shown both theoretically and numerically to possess the same convergence properties as the original problem for all values of the parameter t. We also demonstrated the performance of the a posteriori estimator by applying it successfully to adaptive mesh refinement, and compared the Brinkman model to the Darcy model in the framework of an oil reservoir simulation.

REFERENCES

[1] G. Allaire. Homogenization of the Navier-Stokes equations in open sets perforated with tiny holes. I. abstract framework, a volume distribution of holes. *Arch. Rational Mech. Anal.*, 113(3):209–259, 1990.

[2] G. Allaire. Homogenization of the Navier-Stokes equations in open sets perforated with tiny holes. II. Noncritical sizes of the holes for a volume distribution and a surface distribution of holes. *Arch. Rational Mech. Anal.*, 113(3):261–298, 1990.

[3] T. Arbogast and H. L. Lehr. Homogenization of a Darcy-Stokes system modeling vuggy porous media. *Comput. Geosci.*, 10(3):291–302, 2006.

[4] D. N. Arnold, F. Brezzi, and M. Fortin. A stable finite element for the Stokes equations. *Calcolo*, 21(4):337–344 (1985), 1984.

[5] M. Baudoiun Fraejis de Veubeke. Displacement and equilibrium models in the finite element method. In *Stress analysis, (O.C Zienkiewics and G.S*, pages 145–197. Wiley, 1965.

[6] D. Braess. *Finite Elemente: Theorie, schnelle Löser und Anwendungen in der Elastizitätstheorie. Springer-Verlag.* Springer-Verlag, 1992, 1997.

[7] F. Brezzi, J. Douglas, Jr., R. Durán, and M. Fortin. Mixed finite elements for second order elliptic problems in three variables. *Numer. Math.*, 51(2):237–250, 1987.

[8] F. Brezzi and M. Fortin. *Mixed and Hybrid Finite Element Methods*, volume 15 of *Springer Series in Computational Mathematics*. Springer-Verlag, New York, 1991.

[9] M. A. Christie and M. J. Blunt. Tenth SPE comparative solution project: A comparison of upscaling techniques. *SPE Reservoir Eval. Eng.*, 4(4):308–317, 2001.

[10] B. Cockburn, J. Gopalakrishnan, and R. Lazarov. Unified hybridization of discontinuous Galerkin, mixed, and continuous Galerkin methods for second order elliptic problems. *SIAM J. Numer. Anal.*, 47(2):1319–1365, 2009.

[11] C. D'Angelo and P. Zunino. A finite element method based on weighted interior penalties for heterogeneous incompressible flows. *SIAM Journal on Numerical Analysis*, 47(5):3990–4020, 2009.

[12] H. Egger. A class of hybrid mortar finite element methods for interface problems with non-matching meshes. *AICES-2009-2, Preprint.*

[13] M. Ehrhardt, J. Fuhrmann, and A. Linki. A model of an electrochemical flow cell with porous layer. Preprint 1437, Weierstrass Institute for Applied Analysis and Stochastics, 2009.

[14] E. Gekeler. *Mathematische Methoden zur Mechanik*. Springer-Verlag, Berlin Heidelberg, 2006.

[15] M. Griebel and M. Klitz. Homogenization and numerical simulation of flow in geometries with textile microstructures. *Multiscale Modeling & Simulation*, 8(4):1439–1460, 2010.

[16] A. Hannukainen, M. Juntunen, and R. Stenberg. Computations with finite element methods for the brinkman problem. *Computational Geosciences*, 2010. 10.1007/s10596-010-9204-4.

[17] P. Hansbo and M. Juntunen. Weakly imposed Dirichlet boundary conditions for the Brinkman model of porous media flow. *Applied Numerical Mathematics*, 59(6):1274–1289, 2009.

[18] O. Iliev, R. Lazarov, and J. Willems. Discontinuous galerkin subgrid finite element method for heterogeneous brinkman's equations. In I. Lirkov, S. Margenov, and J. Wasniewski,

editors, *Large-Scale Scientific Computing*, volume 5910 of *Lecture Notes in Computer Science*, pages 14–25. Springer Berlin / Heidelberg, 2010.

[19] M. Juntunen and R. Stenberg. Analysis of finite element methods for the Brinkman problem. *Calcolo*, 2009. DOI:10.1007/s10092-009-0017-6.

[20] G. Kanschat and B. Rivière. A strongly conservative finite element method for the coupling of stokes and darcy flow. *Journal of Computational Physics*, 229(17):5933 – 5943, 2010.

[21] T. Kaya and J. Goldak. Three-dimensional numerical analysis of heat and mass transfer in heat pipes. *Heat and Mass Transfer*, 43:775–785, 2007.

[22] J. Könnö and R. Stenberg. Analysis of H(div)-conforming finite elements for the Brinkman problem. *Helsinki University of Technology Institute of Mathematics Research Report A 582 (2010)*, Submitted for publication.

[23] J. Könnö and R. Stenberg. Non-conforming finite element method for the Brinkman problem. In G. Kreiss, P. Lötstedt, A. Målqvist, and M. Neytcheva, editors, *Numerical Mathematics and Advanced Applications 2009*, pages 515–522. Springer Berlin Heidelberg, 2010.

[24] M. G. Larson and A. Målqvist. A posteriori error estimates for mixed finite element approximations of elliptic problems. *Numer. Math.*, 108(3):487–500, 2008.

[25] T. Lévy. Loi de Darcy ou loi de Brinkman? *C. R. Acad. Sci. Paris Sér. II Méc. Phys. Chim. Sci. Univers Sci. Terre*, 292(12):871–874, Erratum (17):1239, 1981.

[26] C. Lovadina and R. Stenberg. Energy norm a posteriori error estimates for mixed finite element methods. *Math. Comp.*, 75:1659–1674, 2006.

[27] J.-C. Nédélec. A new family of mixed finite elements in $\mathbf{R}^3$. *Numer. Math.*, 50(1):57–81, 1986.

[28] J. Nitsche. Über ein Variationsprinzip zur Lösung von Dirichlet-Problemen bei Verwendung von Teilräumen, die keinen Randbedingungen unterworfen sind. *Abh. Math. Sem. Univ. Hamburg*, 36:9–15, 1971. Collection of articles dedicated to Lothar Collatz on his sixtieth birthday.

[29] P. Popov, Y. Efendiev, and G. Qin. Multiscale modeling and simulations of flows in naturally fractured Karst reservoirs. *Commun. Comput. Phys.*, 6(1):162–184, 2009.

[30] K. R. Rajagopal. On a hierarchy of approximate models for flows of incompressible fluids through porous solids. *Math. Models Methods Appl. Sci.*, 17(2):215–252, 2007.

[31] R. Stenberg. On some techniques for approximating boundary conditions in the finite element method. *J. Comput. Appl. Math.*, 63(1-3):139–148, 1995.

[32] X. Xu and S. Zhang. A new divergence-free interpolation operator with applications to the darcy–stokes–brinkman equations. *SIAM Journal on Scientific Computing*, 32(2):855–874, 2010.

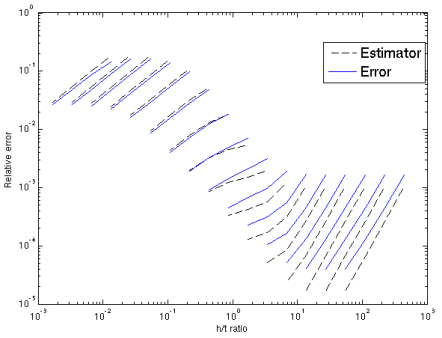

FIGURE 1. *Relative error in the mesh dependent norm. Uniform refinement for a smooth solution* $\beta = 3.1$.

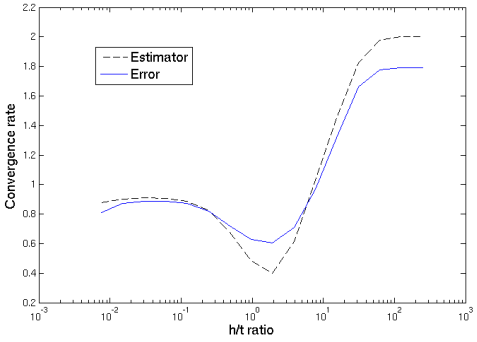

FIGURE 2. *Converge rate for different values of* t. *Uniform refinement for a smooth solution* $\beta = 3.1$.

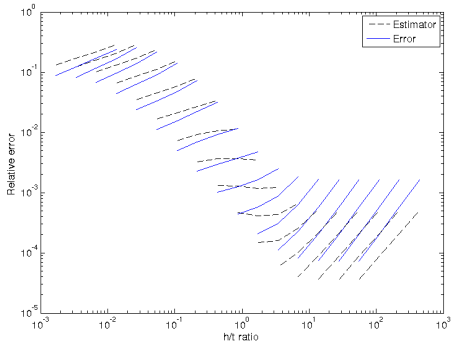

FIGURE 3. *Relative error in the mesh dependent norm. Uniform refinement for an irregular solution* $\beta = 1.52$.

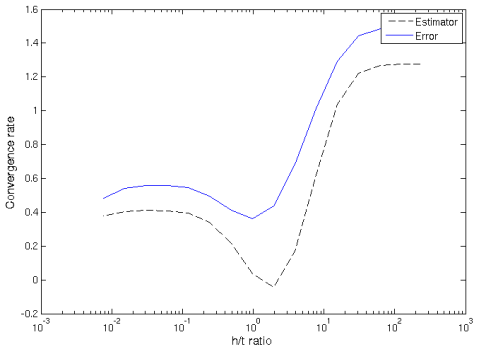

FIGURE 4. *Converge rate for different values of* t. *Uniform refinement for an irregular solution* $\beta = 1.52$.

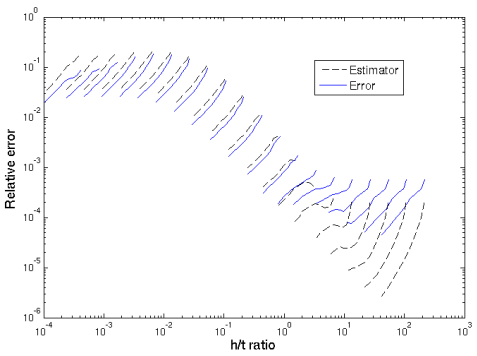

FIGURE 5. *Relative error in the mesh dependent. Adaptive refinement for an irregular solution* $\beta = 1.52$.

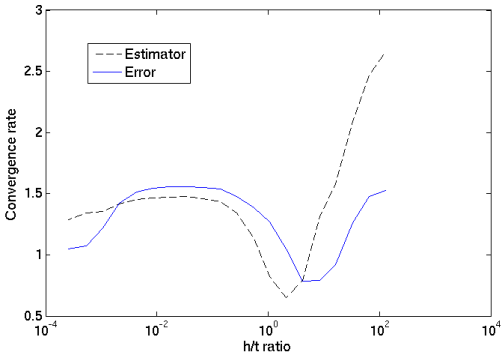

FIGURE 6. *Converge rate for different values of* t. *Adaptive refinement for an irregular solution* $\beta = 1.52$.

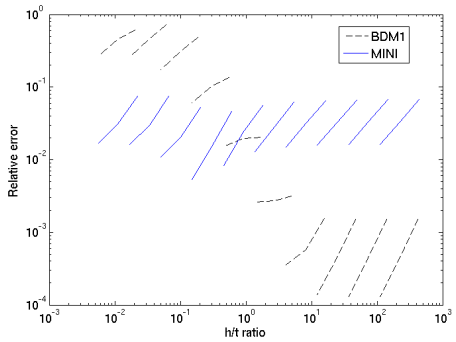

FIGURE 7. *Relative error in the mesh dependent norm. Uniform refinement for a smooth solution* $\beta = 3.1$.

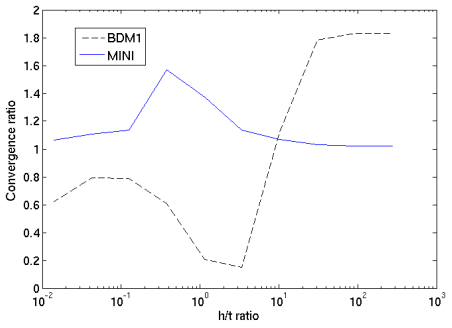

FIGURE 8. *Converge rate for different values of* t. *Uniform refinement for a smooth solution* $\beta = 3.1$.

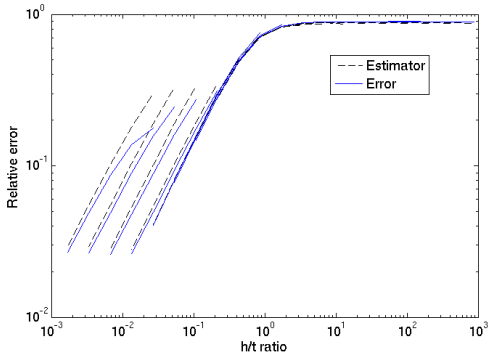

FIGURE 9. *Relative error in the mesh dependent norm without postprocessing. Uniform refinement for a smooth solution* $\beta = 3.1$.

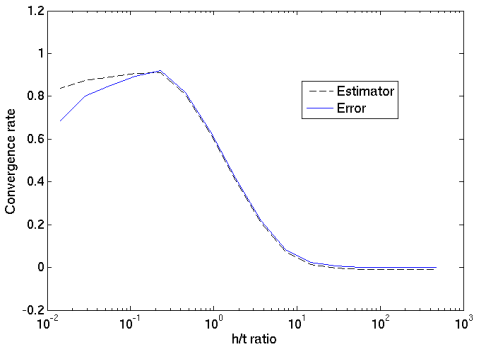

FIGURE 10. *Converge rate for different values of* t *without postprocessing. Uniform refinement for a smooth solution* $\beta = 3.1$.

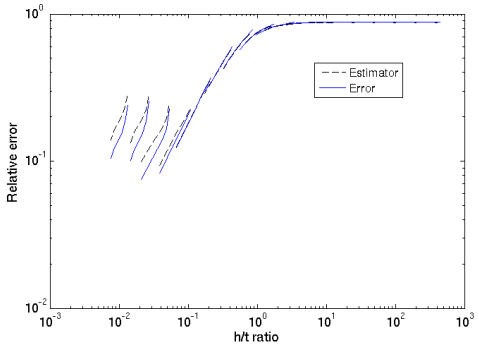

FIGURE 11. *Relative error in the mesh dependent norm without postprocessing. Adaptive refinement for an irregular solution* $\beta = 1.52$.

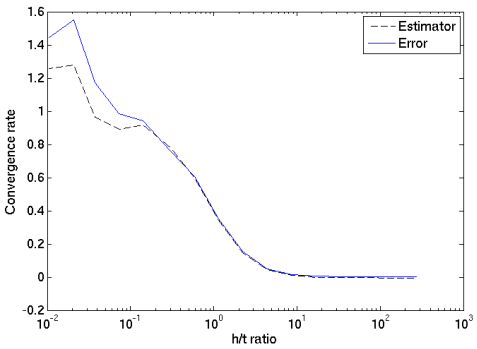

FIGURE 12. *Converge rate for different values of* t *without postprocessing. Adaptive refinement for an irregular solution* $\beta = 1.52$.

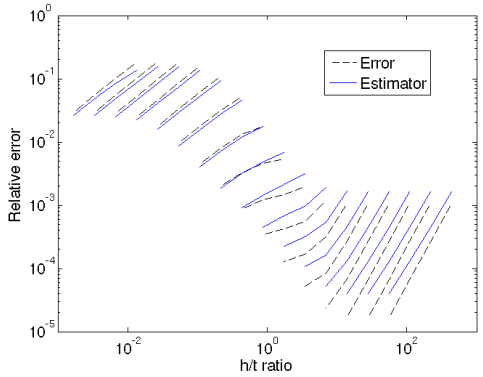

FIGURE 13. *Relative error in the mesh dependent norm for the hybridized method with uniform refinement and* $\beta = 3.1$.

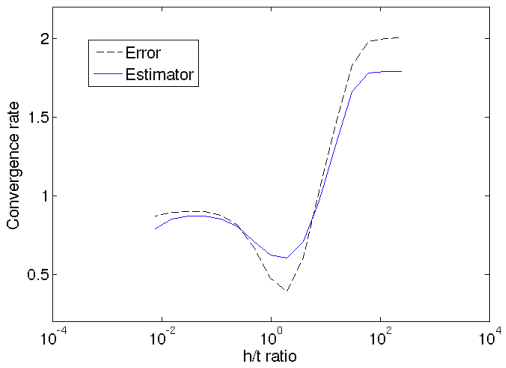

FIGURE 14. *Converge rate for different values of* t *for the hybridized method with* $\beta = 3.1$.

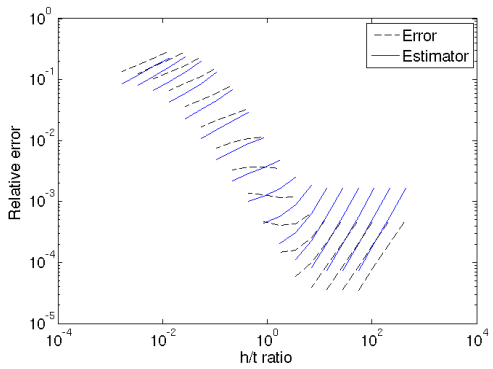

FIGURE 15. *Relative error in the mesh dependent norm for the hybridized method with uniform refinement and* $\beta = 1.52$.

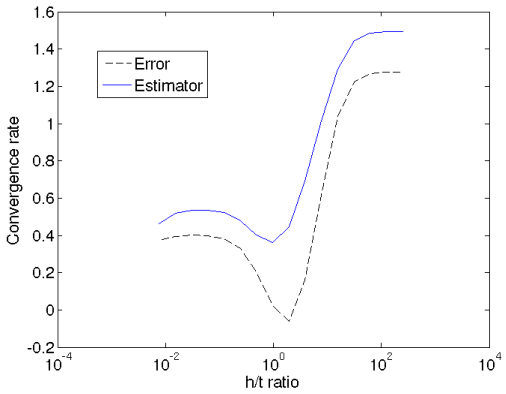

FIGURE 16. *Converge rate for different values of* t *for the hybridized method with* $\beta = 1.52$.

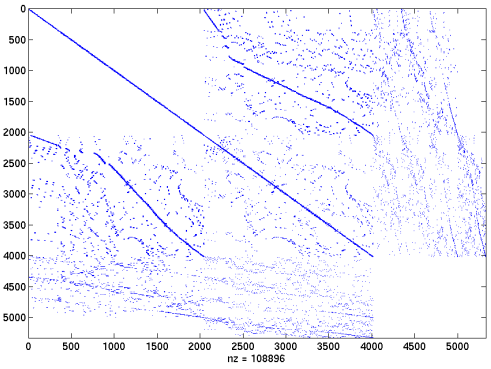

FIGURE 17. *Sparsity pattern of the system matrix for the standard method.*

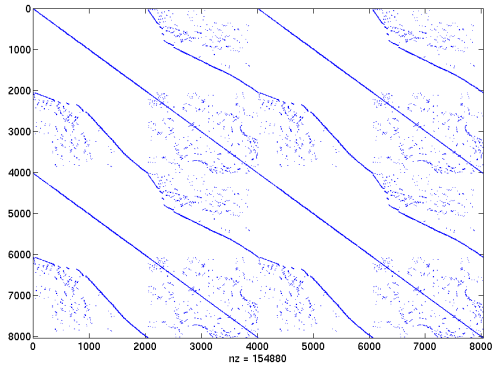

FIGURE 18. *Sparsity pattern of the system matrix for the hybridized version.*

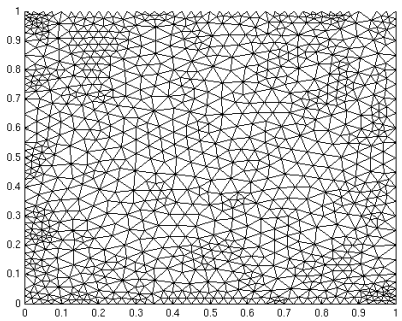

FIGURE 19. *Final mesh after adaptive refinement,* $t = 0.5$

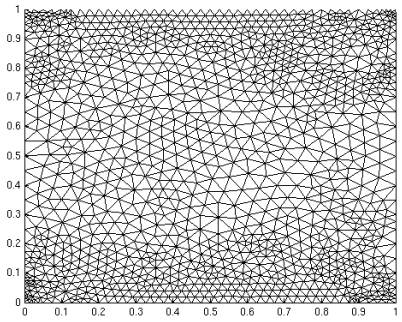

FIGURE 20. *Final mesh after adaptive refinement,* $t = 0.2$

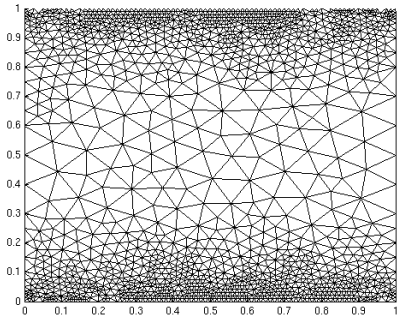

FIGURE 21. *Final mesh after adaptive refinement,* $t = 0.1$

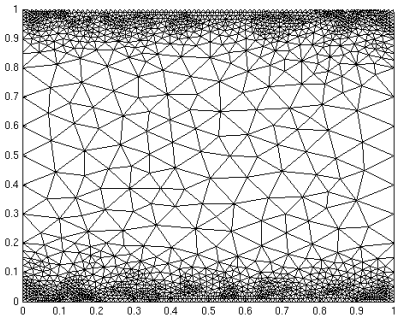

FIGURE 22. *Final mesh after adaptive refinement,* $t = 0.05$

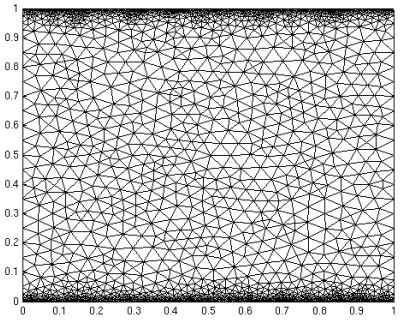

FIGURE 23. *Final mesh after adaptive refinement,* $t = 0.005$

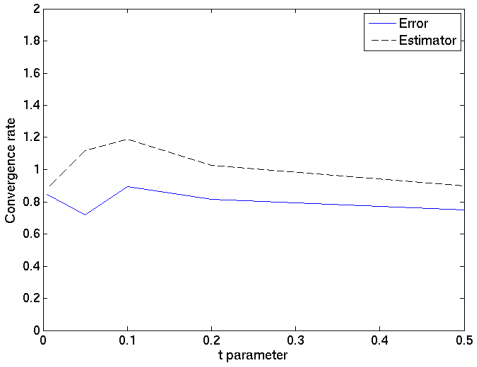

FIGURE 24. *Convergence rates of the adaptive solution for different values of* t.

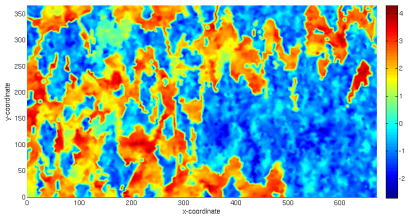

FIGURE 25. *Average of the logarithm of the permeability tensor diagonal components in mD. Layer 68 of the SPE10 model, median of the permeability is* 0.428 *mD.*

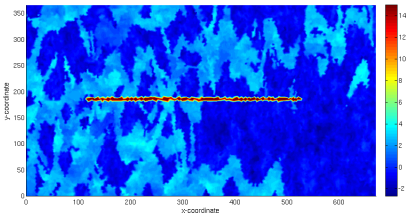

FIGURE 26. *Average of the logarithm of the permeability tensor diagonal components in mD. Layer 68 of the SPE10 model with an added permeability streak of* 10^{12} *D.*

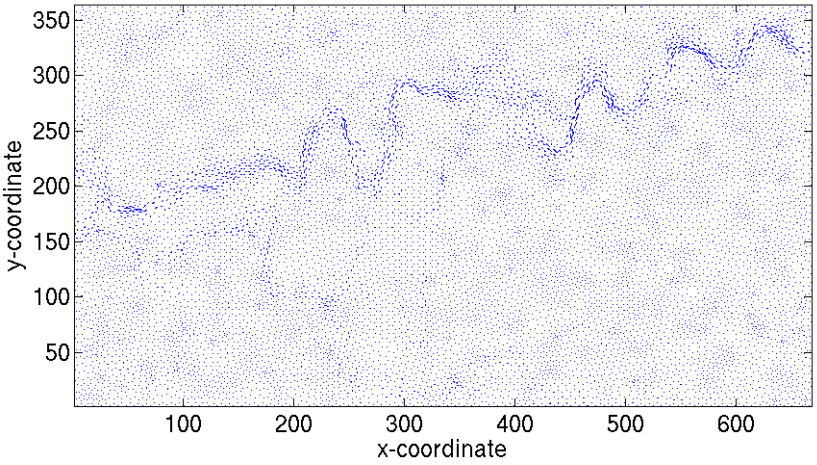

FIGURE 27. *Flow for the original model.*

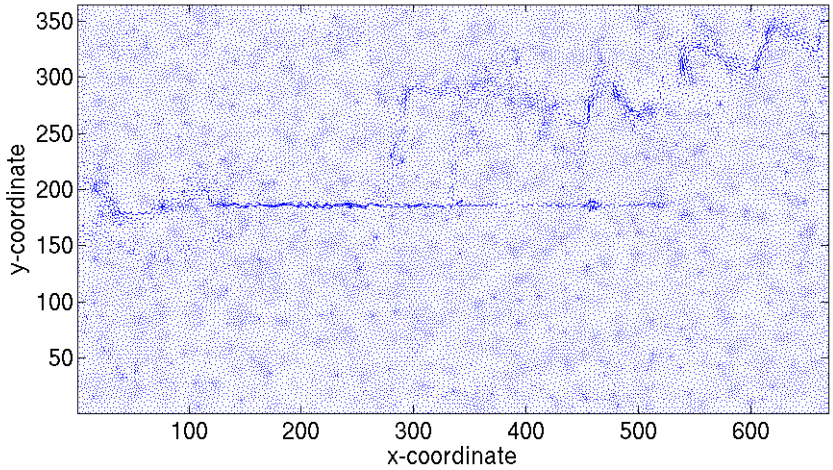

FIGURE 28. *Flow for the modified model with streak permeability of* 10^{12} *D.*

(continued from the back cover)

A589 Antti Rasila, Jarno Talponen
Convexity properties of quasihyperbolic balls on Banach spaces
August 2010

A588 Kalle Mikkola
Real solutions to control, approximation, factorization, representation, Hankel and Toeplitz problems
June 2010

A587 Antti Hannukainen, Rolf Stenberg, Martin Vohralík
A unified framework for a posteriori error estimation for the Stokes problem
May 2010

A586 Kui Du, Olavi Nevanlinna
Minimal residual methods for solving a class of R-linear systems of equations
May 2010

A585 Daniel Aalto
Boundedness of maximal operators and oscillation of functions in metric measure spaces
March 2010

A584 Tapio Helin
Discretization and Bayesian modeling in inverse problems and imaging
February 2010

A583 Wolfgang Desch, Stig-Olof Londen
Semilinear stochastic integral equations in L_p
December 2009

A582 Juho Könnö, Rolf Stenberg
Analysis of H(div)-conforming finite elements for the Brinkman problem
January 2010

A581 Wolfgang Desch, Stig-Olof Londen
An L_p-theory for stochastic integral equations
November 2009

HELSINKI UNIVERSITY OF TECHNOLOGY INSTITUTE OF MATHEMATICS
RESEARCH REPORTS

The reports are available at *http://math.tkk.fi/reports/* .
The list of reports is continued inside the back cover.

A594 Atte Aalto, Jarmo Malinen
Cauchy problems from networks of passive boundary control systems
October 2010

A593 Toni Lassila
Model reduction and level set methods for shape optimization problems
October 2010

A592 Olavi Nevanlinna
Upper bounds for $\mathbb{R}$-linear resolvents
September 2010

A591 Juhana Siljander
Regularity for degenerate nonlinear parabolic partial differential equations
September 2010

A590 Ehsan Azmoodeh
Riemann-Stieltjes integrals with respect to fractional Brownian motion and applications
September 2010

ISBN 978-952-60-3511-6 (print)
ISBN 978-952-60-3512-3 (PDF)
ISSN 0784-3143 (print)
ISSN 1797-5867 (PDF)